REAL-TIME VIRTUAL ANALOG MODELLING OF DIODE-BASED VCAs

Coriander V. Pines

Independent researcher
Boston, MA, USA
`hello@corianderpines.org`

ABSTRACT

Some early analog voltage-controlled amplifiers (VCAs) utilized semiconductor diodes as a variable-gain element. Diode-based VCAs exhibit a unique sound quality, with distortion dependent both on signal level and gain control. In this work, we examine the behavior of a simplified circuit for a diode-based VCA and propose a nonlinear, explicit, stateless digital model. This approach avoids traditional iterative algorithms, which can be computationally intensive. The resulting digital model retains the sonic characteristics of the analog model and is suitable for real-time simulation. We present an analysis of the gain characteristics and harmonic distortion produced by this model, as well as practical guidance for implementation. We apply this approach to a set of alternative analog topologies and introduce a family of digital VCA models based on fixed nonlinearities with variable operating points.

1. INTRODUCTION

Voltage-controlled amplifiers (VCAs) are a fundamental building block of audio processing and synthesis. They are used in a wide array of applications, such as compressors, expanders, limiters, synthesizer envelopes, and dynamic filters. VCAs are also used to perform mixing, amplitude modulation, and gating [1].

VCAs can be trivial to implement in the digital domain, requiring only a single multiplication at their simplest. Analog VCAs are significantly more complex, and have been implemented in many ways as technology has progressed, using components such as LDRs, vacuum tubes, semiconductor diodes, BJTs, JFETs, and OTAs [2, 3]. Each topology creates a unique sound, which is influenced by distortion characteristics, control linearity, and time-dependent effects.

Some of the earliest solid-state compressors and limiters, introduced in the 1960s, used semiconductor diodes as their primary variable-gain elements; notable examples include the Siemens U273 Limiter [4], the Dolby Audio Noise Reduction System A301 [5], the Neve 2254/E Limiter/Compressor [6], and the Neve 33609/J Limiter/Compressor [7]. With a few exceptions, diode-based VCAs are nearly non-existent in modern products, likely owing to their relatively high signal distortion, need for carefully matched components, temperature dependence, and higher noise floor.

While the designers of historic analog systems sought to minimize distortion, today the nonlinearities and quirks present in analog hardware are appreciated for their musical effects [8], and work in virtual analog modelling is widely undertaken. Though diode simulations have been employed in digital effects such as
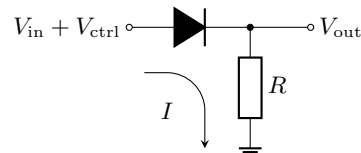
Figure 1: *Analog circuit prototype for a diode-resistor VCA.*

distortion [9, 10, 11, 12, 13] and ring modulation [14, 15], a careful review of prior literature did not reveal any existing digital models of diode-based VCAs. In this work, we propose a family of generalized models based on different diode-based VCA topologies.

2. ANALOG CIRCUIT PROTOTYPE

Fig. 1 depicts the circuit that will serve as a prototype for our development of a digital diode VCA model: V_{in} summed with V_{ctrl} is connected to ground through a forward-biased diode and resistor in series, and V_{out} is taken across the resistor. Though this circuit omits many support components required in a practical diode-based VCA (e.g., buffering, AC coupling, and gain staging), it is sufficient to develop a digital model.

The circuit forms a voltage divider in which the diode behaves like a voltage-dependent resistor. Current flow through the circuit is governed by the Shockley diode equation and Kirchhoff's current law, and obeys the equation

$$I_{\text{S}} \exp\left(\frac{V_{\text{in}} + V_{\text{ctrl}} - V_{\text{out}}}{\eta V_{\text{T}}} \right) - I_{\text{S}} - \frac{V_{\text{out}}}{R} = 0 , \qquad (1)$$

where I_{S} is the diode's reverse-bias saturation current, η is the diode's ideality factor, and V_{T} is the thermal voltage. The model in (1) is an approximation, and excludes some properties of physical semiconductor diodes, namely: internal resistance, inductance, and capacitance*; noise†; and the reverse-recovery effect [16]. As these effects are largely below the threshold of audibility, we ignore them for the purposes of analysis. Reverse breakdown is also disregarded, as it typically occurs at voltages greater than those present in audio processing equipment. All models and analysis assume a fixed temperature, and the effects of temperature variation are not modelled.

---

*Internal capacitance somewhat increases the gain of high-frequency components when the overall gain is low; if desired, this effect can be simulated in a digital model with a variable high-boost filter.

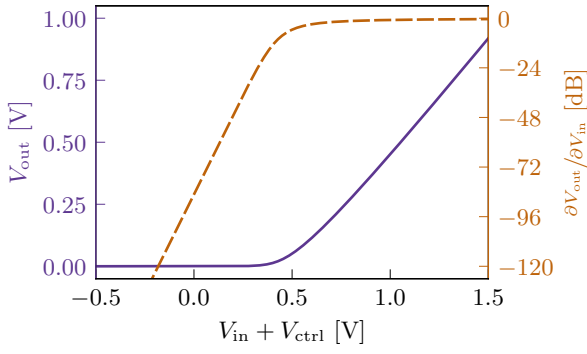†Likewise, simulated noise dependent on signal level and gain can be applied to the output to approximate this effect.

Figure 2: *DC signal sweep (solid) and small-signal gain (dashed) for the diode-resistor VCA circuit in Fig. 1, with $R = 1\,\text{k}\Omega$ and $I_S = 2.520\,\text{nA}$, $\eta = 1.755$, and $V_T = 25.85\,\text{mV}$ corresponding to a 1N4148 diode at $300\,\text{K}$.*

As illustrated in Fig. 2, the circuit in Fig. 1 behaves like a *soft rectifier* with regard to $V_\text{in} + V_\text{ctrl}$, broadly permitting voltage to flow in the forward direction while blocking it in the reverse direction. The width of the transition region between conduction and blocking is proportional to ηV_T.

We decompose the input voltage into two components: the input signal V_in and the control voltage V_ctrl. The input signal is assumed to have no DC component, and its magnitude is kept relatively small (nominally below $50\,\text{mV}_\text{PP}$ in commercial products). The control voltage sets the circuit's DC operating point and ultimately determines the gain applied to the input signal. As $V_\text{ctrl} \to +\infty\,\text{V}$, the diode behaves like a short circuit and the gain approaches unity. Conversely, as $V_\text{ctrl} \to -\infty\,\text{V}$, the diode behaves like an open circuit and the gain approaches zero.

The input signal V_in is predominantly affected by the circuit's small-signal characteristics. The small-signal gain may be computed exactly by implicitly differentiating (1) and performing algebraic manipulation to obtain

$$\frac{\partial V_\text{out}}{\partial V_\text{in}} = \frac{V_\text{out} + I_S R}{V_\text{out} + I_S R + \eta V_T}, \tag{2}$$

also shown in Fig. 2. The small-signal gain is a function of the circuit's DC operating point; it is this property that we will exploit to create a variable gain element. Note that a DC offset is present at the output due to V_ctrl. This offset is referred to as control voltage feedthrough, and typically removed using AC coupling.

The usual iterative algorithms may be used to solve for V_out in the digital domain; however, these methods are often computationally intensive. Instead, we seek an explicit solution. This also makes translation to a DSP model more straightforward. An exact analytical expression for the output voltage may be obtained in terms of the Lambert W function [17] using the method described in [18]. Because $I_S R/\eta V_T \geq 0$, the argument of $W()$ is positive and thus there is exactly one solution, given by the principal branch

$$V_\text{out} = \eta V_T\, W_0\left(\frac{I_S R}{\eta V_T} \exp\left(\frac{V_\text{in} + V_\text{ctrl} + I_S R}{\eta V_T}\right)\right) - I_S R. \tag{3}$$

3. DSP MODEL

Because (3) does not contain any dynamic terms, we may transform it into a stateless DSP model by a series of substitutions.

To begin, we replace $W_0()$ with the Wright omega function [19], defined here as $\omega(u) = W_0(e^u)$, to obtain

$$V_\text{out} = \eta V_T\, \omega\left(\frac{V_\text{in} + V_\text{ctrl} + I_S R}{\eta V_T} + \ln\left(\frac{I_S R}{\eta V_T}\right)\right) - I_S R,$$

which we further simplify using the identity $\omega^{-1}(u) = u + \ln u$ to

$$V_\text{out} = \eta V_T\, \omega\left(\frac{V_\text{in} + V_\text{ctrl}}{\eta V_T} + \omega^{-1}\left(\frac{I_S R}{\eta V_T}\right)\right) - I_S R. \tag{4}$$

The Wright omega function is preferable here for several reasons: it is defined over the entire real line, has a number of convenient algebraic properties, is more efficient and stable under numerical evaluation for large values, and can be approximated more simply. In particular, the function can be directly mapped onto a diode-resistor VCA's voltage transfer function using only affine transformations. A great number of published algorithms and approximations, including [9, 10, 14, 15, 20], have been proposed for evaluating the Lambert W and Wright omega functions, each of which trade performance for accuracy to varying degrees. Additionally, the omega function is monotonic, which makes it well-suited to tabulation. When preparing this work, we used [9, (12)] for real-time evaluation and [20] for plots and offline processing.

Next, we introduce two control-rate parameters that divorce the model from physical component values and provide a more natural parameterization. The *sharpness parameter* $\alpha := (\eta V_T)^{-1}$ determines the transition region sharpness and affects the model's degree of nonlinearity. In an analog circuit, α is necessarily positive; in the digital domain, we may permit $\alpha \in \mathbb{R}$ without issue. The *bias parameter* $\beta := V_\text{ctrl}/\eta V_T + \omega^{-1}(I_S R/\eta V_T)$ sets the model's operating point. Similarly, we allow $\beta \in \mathbb{R}$. This particular expression was chosen to decouple the bias and sharpness parameters. In Sec. 3.1 we will discuss the exact relationship between β and the small-signal gain. To avoid discontinuities, α and β should ideally be changed only when x crosses zero.

We also rename $x := V_\text{in}$ and $y := V_\text{out}$. For the sake of later analysis, we will assume that the input signal x has no DC component. After substitution, we arrive at

$$y(x) = \alpha^{-1}\omega(\alpha x + \beta) - \alpha^{-1}\omega\left(\beta - \frac{V_\text{ctrl}}{\eta V_T}\right).$$

Lastly, we alter the model by removing the $-V_\text{ctrl}/\eta V_T$ term, eliminating the DC offset such that $y(0) = 0$. Removing this term also minimizes audible "thumping" that can be produced when β is rapidly modulated; we will discuss this phenomenon in further detail in Sec. 4.3. This alteration does not affect the distortion characteristics of the model with regard to the input signal. We now arrive at the expression

$$y(x) = \alpha^{-1}\omega(\alpha x + \beta) - \alpha^{-1}\omega(\beta), \tag{5}$$

which is shown in Fig. 3 for various values of β.

Compared to traditional iterative solvers, (5) is computationally efficient. It requires only two additions, two multiplications, and one $\omega()$ evaluation per sample for constant parameters; therefore it may readily be evaluated in real-time on modern computers and embedded processors.
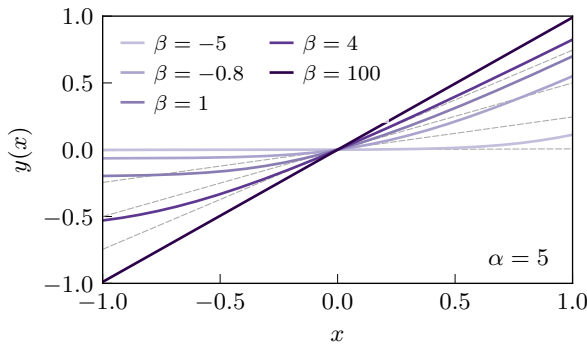
Figure 3: *Input signal sweeps of* (5) *for* β *values corresponding to small-signal gains of approximately 1%, 25%, 50%, 75%, and 99%. Dashed lines indicate linear functions with equivalent gain.*

3.1. Gain Control

In order to make (5) usable as a VCA, we must parameterize β in terms of the model's gain. We compute the small-signal gain A for vanishingly small input signals,

$$A := \lim_{\alpha \to 0} \frac{\partial y}{\partial x} = \omega'(\beta) = \frac{\omega(\beta)}{\omega(\beta) + 1} . \tag{6}$$

A is wholly dependent on the bias parameter β: as $\beta \to +\infty$, A approaches unity; likewise, as $\beta \to -\infty$, the small-signal gain approaches zero. By inverting (6), we arrive at the gain control parameterization,

$$\beta(A) = \omega^{-1}\left(\frac{A}{1 - A}\right), \tag{7}$$

which is defined on the open interval $A \in (0, 1)$ and may be evaluated using $\omega^{-1}(u) = u + \ln u$. Modulating β is comparatively expensive, requiring two additions, one division, and one $\ln()$ evaluation. Some effort may be saved when computing the $-\alpha^{-1}\omega(\beta)$ term in (5) by observing that $\omega(\beta) = A/(1 - A)$. Tabulation may also be used to compute (7).

The results in (6) and (7) make use of $\omega'(u) = \omega(u)/(\omega(u) + 1)$; it is worth noting that not all approximations of the Wright omega function obey this identity exactly, and may thus require different gain control parameterizations.

3.2. Comparison to SPICE Simulations

When parameters are matched, (5) produces a response nearly indistinguishable (when corrected for DC offset) from a SPICE simulation of the circuit in Fig. 1, as shown in Fig. 4. The region of greatest relative error occurs when gain is near zero, resulting in diminished impact. As a static system, the model's accuracy is independent of input frequency and sampling rate.

3.3. Analysis of Harmonic Distortion

The system described by (5) is static and thus does not modify phase. Instead, the particular sound qualities of diode-based VCAs are largely due to gain-dependent distortion.
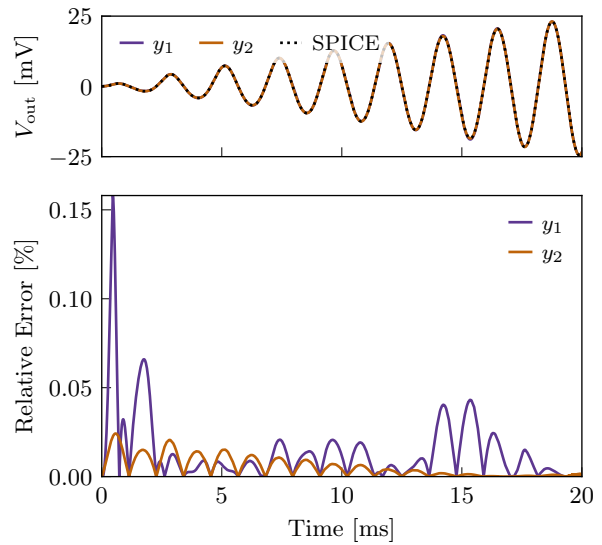

Figure 4: *Time domain waveforms (top) and relative errors (bottom) comparing* (5) *to a SPICE simulation of Fig. 1 with* $R = 1\,\text{k}\Omega$ *and* $I_\text{S} = 2.520\,\text{nA}$, $\eta = 1.755$, *and* $V_\text{T} = 25.85\,\text{mV}$ *corresponding to a 1N4148 diode at* $300\,\text{K}$. *The input is a* $50\,\text{mV}_\text{PP}$ $440\,\text{Hz}$ *sine sampled at* $48\,\text{kHz}$. A *is linearly swept from 0 to 1 over the run duration. Trace* y_1 *uses [9, (12)] to evaluate* $\omega()$, *while* y_2 *uses the algorithm described in [20]. The DC offset has been removed from the SPICE simulation trace.*

The magnitude and sign of a given harmonic h_n produced for a sinusoidal input $x = \cos(2\pi f t)$ follows from the Fourier series expansion of $y(x)$ and is given by

$$h_n = \frac{2}{\pi\alpha} \int_0^\pi \cos(nu)\,\omega(\alpha\cos(u) + \beta)\,du \tag{8}$$

for $n \in \mathbb{N}^*$, such that $y(x) = c + \sum_{n \geq 1} h_n \cos(2\pi n f t)$. An exact analytical solution for h_n cannot be expressed in terms of elementary functions. The harmonic level plots shown in this work were obtained by evaluating (8) numerically via the DCT using the algorithm in [20] to evaluate $\omega()$. One may also approximate the integral analytically using one of the series expansions given in [19] for those values of α and β which permit convergence.

Both α and β affect the amount of harmonic distortion introduced by the model. Because the input signal x is always multiplied by α, changing the input signal magnitude is equivalent to changing α by a corresponding amount; thus, we will frame the effects of input signal magnitude solely in terms of α. When $\alpha \approx 0$, $y(x) \approx Ax$ for all values of β, and thus the model is largely indistinguishable from a perfect digital VCA. As $|\alpha|$ increases, harmonic distortion increases in turn. The sign of α affects the signs of even harmonics, but not their magnitude.

As $\beta \to +\infty$ (*i.e.*, A approaches unity), the curve becomes increasingly linear and total harmonic distortion decreases, even for larger values of $|\alpha|$. Conversely, as $\beta \to -\infty$ (*i.e.*, A approaches zero), the curve becomes less linear and the total harmonic dis-
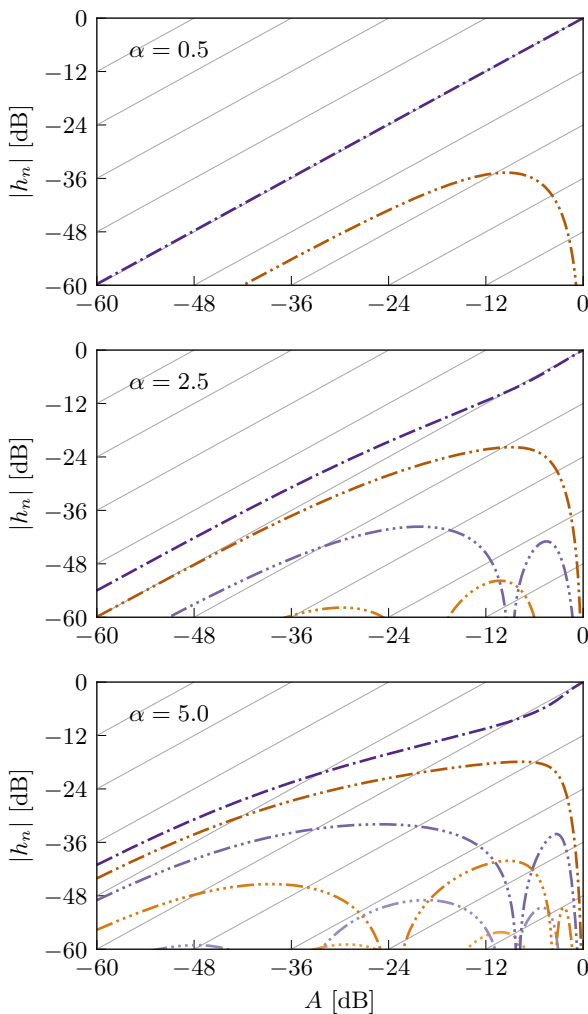
Figure 6: *RMS of output compared to input for a compensated model combining* (9) *and* (10), *showing various values of* γ. *The input is* $x = \cos(t)$ *sampled at* $5\,\mathrm{kHz}$ *for a duration of* $1\,\mathrm{s}$. *Dashed line indicates the ideal linear gain response.*

4. IMPLEMENTATION CONSIDERATIONS

4.1. Signal Contribution to Effective Gain

When $|\alpha|$ is relatively large, the input signal can shift the operating point away from β by a significant degree. This can cause the effective gain, defined here as $\mathrm{RMS}\{y\}/\mathrm{RMS}\{x\}$, to differ from the small-signal gain. This disparity is especially prevalent when $\alpha x > 0$ due to the shape of (6). In this region, a significant portion of the input signal can pass through the VCA even for values of A close to zero; we refer to this phenomenon as gain parameter overestimation. This behavior can be clearly seen in the third row of Fig. 5.

In applications where accurate gain tracking is required, we suggest modifying (5) by subtracting some portion of α from β,

$$y^\star(x) = \alpha^{-1}\omega(\alpha x + \beta - \gamma|\alpha|) - \alpha^{-1}\omega(\beta - \gamma|\alpha|) \quad (9)$$

where $\gamma \in [0, 1]$ sets the amount of compensation to apply. The optimal value for γ depends only on $|\alpha|$; it approaches 0 as $|\alpha| \to 0$ and 1 as $|\alpha| \to \infty$, though we were unable to determine the exact relationship between the two parameters.

4.2. Bias Parameter Magnitude

The expression (7) has non-removable singularities that prevent the model from attaining zero or unity gain, as $\lim_{A\to 0^+} \beta(A) = -\infty$ and $\lim_{A\to 1^-} \beta(A) = +\infty$. This problem is further compounded by floating point rounding errors: when $|\beta| \gg |\alpha|$ and $x \sim U(-1, 1)$, the expression $\alpha x + \beta$ introduces an average of $\log_2|\beta| - \log_2|\alpha| + 2$ bits of rounding error. Given that IEEE 754 single-precision floats carry 24 bits of significand precision, rounding errors can quickly become audible as $|\beta|$ increases. We therefore seek to place constraints on the value of β. Because this in turn limits the available range of A, (5) and (7) must be modified to compensate. We may instead use

$$A^\star = \max(A, A_{\min}), \quad (10a)$$

$$y^\star(x) = \frac{A}{A^\star}\frac{1+\epsilon}{\alpha}\big(\omega(\alpha x + \beta^\star) - \omega(\beta^\star)\big), \quad (10b)$$

$$\beta^\star(A^\star) = \omega^{-1}\left(\frac{A^\star}{1+\epsilon - A^\star}\right), \quad (10c)$$

Figure 5: *Magnitude of harmonics introduced by* (5) *when applied to* $x = \cos(2\pi f t)$, *relative to the input signal. The frequency multiple* n *is indicated by the number of dots; odd harmonics are purple and even harmonics are orange. Grey grid lines show* $20\,\mathrm{dB}$ *per decade slopes.*

tortion *increases*[‡]. This inverse relationship is somewhat counterintuitive compared to other waveshaping models, which typically exhibit increased distortion with increased gain.

Fig. 5 shows the relative level of each harmonic multiple introduced when (5) is applied to a sinusoidal input. The odd and even harmonics produced by the model tend to cluster in lobes; for some gain settings, even harmonics dominate (resulting in a "warmer" sound), while at other settings, odd harmonics are more pronounced (resulting in a more "metallic" sound). This lends the model a dynamic and shifting timbre with the potential to add auditory interest to synthesizers and effects.

[‡]A rigorous proof is beyond the scope of this paper, but the behavior can be seen by observing that the extrinsic curvature κ of $y(x)/y'(x)$, evaluated at $x = 0$, decreases monotonically as β increases.

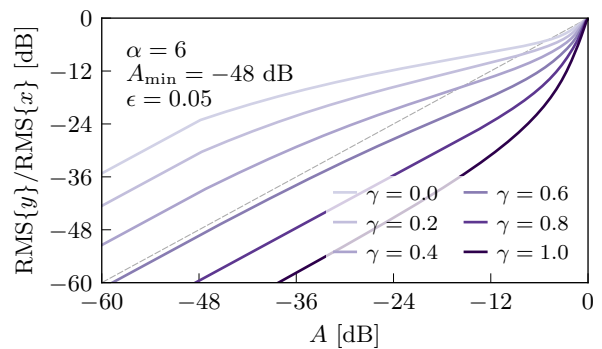where $\epsilon \geq 0$ and $A_{\min} \geq 0$ are small values. This allows for $A \in [0, 1]$. The parameter ϵ moves the pole in (10c) outside the range of $A^\star$, and $A_{\min}$ establishes the minimum gain effected by the VCA model; when $A < A_{\min}$, the output signal is linearly scaled to compensate, which additionally mitigates gain parameter overestimation. These modifications impose the constraint $\beta^\star \in [\beta^\star(A_{\min}), \omega^{-1}(\epsilon^{-1})]$ while allowing for $A \in [0, 1]$ without significantly changing the model's characteristics. The parameters need not be large; in fact, setting $\epsilon = 0.02$ and $A_{\min} = 0.001$ limits $\beta \in [-6.9, 53.9]$ and produced indistinguishable results in informal listening tests.

Fig. 6 illustrates the gain characteristics of a compensated model combining (9) and (10).

4.3. DC Blocking

Adding DC blocking filters to the VCA model's input and output is strongly recommended. Any DC offset present at the input effectively contributes to β and changes the system's gain in the same manner as described in Sec. 4.1.

Because the Wright omega function is asymmetric, some DC components are present at the output that are not completely removed by the $-\alpha^{-1}\omega(\beta)$ term. Note that an output DC blocking filter does not completely obviate the need for this term; without it, rapid gain modulation can produce audible "thumping" at the output that can pass through a DC blocking filter.

4.4. Antialiasing

The Wright omega function is nonlinear and thus can generate harmonic components above a system's Nyquist frequency. These components appear in the output signal as aliasing distortion, which is often undesirable.

Upsampling $\alpha x + \beta$ before evaluating the nonlinearity greatly reduces aliasing by raising the effective Nyquist frequency at the expense of increased $\omega()$ evaluations per sample. Large values of $|\alpha|$ introduce more distortion and therefore suggest the use of higher oversampling factors. The degree of oversampling necessary to render aliasing inaudible is relatively low; despite the magnitude of harmonics relative to the output signal *increasing* as $A \to 0$, the absolute magnitude of each harmonic *decreases*.

The antiderivative antialiasing (ADAA) technique described in [21] is particularly well-suited to this model, and may be applied instead of or in conjunction with oversampling. This is due to the property that antiderivatives of $\omega()$ are polynomial functions of $\omega()$ itself. Namely,

$$\int \omega(u)\, du = \frac{1}{2}\omega^2(u) + \omega(u) + C\,,$$

$$\int u\,\omega(u)\, du = -\frac{1}{6}\omega^3(u) + \left(\frac{1}{2}u - \frac{3}{4}\right)\omega^2(u)$$
$$+ (u - 1)\,\omega(u) + C\,.$$

Comparisons of the antialiasing methods described in this section, as well as other methods using matched filters, may be found on the companion page to this paper§.
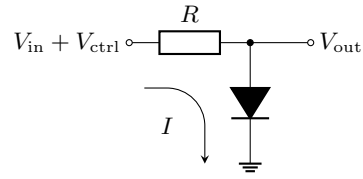

Figure 7: *Analog circuit prototype for resistor-diode VCA obtained by interchanging the diode and resistor in Fig. 1.*

5. TOPOLOGICAL VARIATIONS

5.1. Quasi-Logarithmic Converter

A topological variation may be found by interchanging the diode and resistor in Fig. 1 such that V_{out} is taken across the diode rather than the resistor, as shown in Fig. 7. This circuit is often called a logarithmic converter [22], as its response approximates a logarithmic curve for large input values.

An expression for V_{out} may be derived from (4) by observing that the voltages across the diode and resistor must necessarily sum to V_{in}; hence,

$$V_{\text{out}} = V_{\text{in}} - \eta V_{\text{T}}\, \omega\left(\frac{V_{\text{in}} + V_{\text{ctrl}}}{\eta V_{\text{T}}} + \omega^{-1}\left(\frac{I_{\text{S}} R}{\eta V_{\text{T}}}\right)\right) + I_{\text{S}} R\,. \tag{11}$$

By extension, we derive the DSP model for this topology by subtracting (5) from x such that

$$y(x) = x - \alpha^{-1}\omega(\alpha x + \beta) + \alpha^{-1}\omega(\beta)\,, \tag{12a}$$

$$A = \frac{1}{\omega(\beta) + 1}\,, \tag{12b}$$

$$\beta(A) = \omega^{-1}\left(\frac{1 - A}{A}\right)\,, \tag{12c}$$

where (12c) is defined on the open interval $A \in (0, 1)$. This form more readily demonstrates why the circuit in Fig. 7 is called a logarithmic converter: $\omega(\alpha x) + \ln(\omega(\alpha x)) = \alpha x$ by definition; thus $x - \alpha^{-1}\omega(\alpha x) = \alpha^{-1}\ln(\omega(\alpha x)) \approx \alpha^{-1}\ln(\alpha x)$ for large positive values of αx. In contrast with $\ln()$, (12a) is real and finite for all $x \in \mathbb{R}$.

The signal sweep and harmonic distortion introduced by (12a) are shown in Column (a) of Fig. 8. Unlike (5) which approaches a linear function as $A \to 1$, this model's response curve approaches linearity as $A \to 0$. This results in peak distortion near unity gain, which rapidly decreases as the gain decreases; indeed, the harmonics introduced by this model fall off at approximately 40 dB per decade as the gain parameter approaches zero. By keeping the gain parameter below some predetermined threshold and applying sufficient make-up gain, distortion can be reduced until it is largely inaudible. Additionally, the gain parameter overestimation problem described in Sec. 4.1 is less pronounced in this model, occurring when the gain parameter is near unity rather than near zero. For these reasons, commercial diode-based VCAs sometimes prefer designs that build on this topology [2, 5, 7].
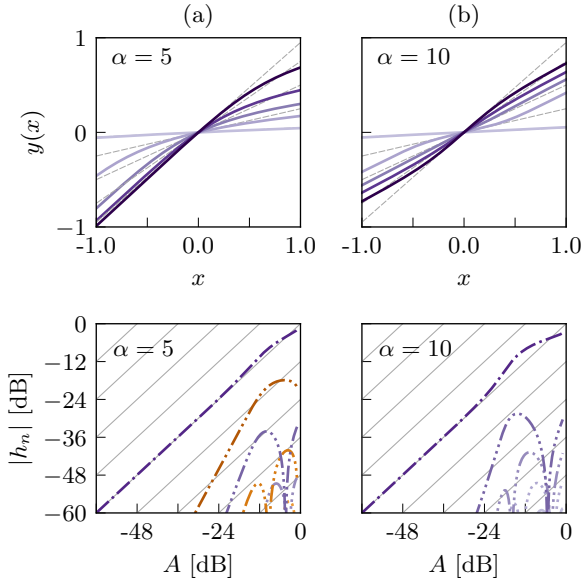
Figure 8: *Topological variations from left to right: (a) Quasi-Logarithmic Converter, Sec. 5.1; (b) Current-Controlled Bridge, Sec. 5.2. Top row: Input signal sweeps of each model for various values of β. Dashed lines indicate linear functions with equivalent gain. Bottom row: relative harmonic levels introduced by each model when applied to a sinusoidal input signal $x = \cos(2\pi f t)$. The frequency multiple is indicated by the number of dots; odd harmonics are purple and even harmonics are orange. Grey grid lines show 20 dB per decade slopes.*

5.2. Current-Controlled Bridge

The circuit described in Sec. 5.1 can be altered to control the gain using a control current rather than a control voltage. Two resistor-diode VCAs may also be placed in parallel to construct a symmetric bridge. The Dolby A301 Audio Noise Reduction System [5], a multi-band companding processor released in 1966, utilized this topology in its VCA sections, implementing a voltage-controlled current source/sink using a pair of BJTs.

Fig. 9 depicts a simplified version of a current-controlled resistor-diode bridge VCA. This circuit is described by the equations

$$\frac{V_{\text{in}} - V_{\text{a}}}{R_1} + I_{\text{S}} \exp\left(\frac{V_+ - V_{\text{a}}}{\eta V_{\text{T}}}\right) - I_{\text{S}} - I_{\text{ctrl}} = 0, \quad (13\text{a})$$

$$\frac{V_{\text{in}} - V_{\text{b}}}{R_1} - I_{\text{S}} \exp\left(\frac{V_{\text{b}} - V_-}{\eta V_{\text{T}}}\right) + I_{\text{S}} + I_{\text{ctrl}} = 0, \quad (13\text{b})$$

$$V_{\text{out}} = \frac{V_{\text{a}} + V_{\text{b}}}{2}. \quad (13\text{c})$$

Without loss of generality, we impose the constraint $V_- = -V_+$[¶]. The Wright omega function can again be used to obtain

---

[¶]Unequal supply voltages $V_- \neq -V_+$ apply a DC offset of $1/2 V_+ + 1/2 V_-$ to V_{in}, V_{out}, and $I_{\text{ctrl}} R_1$, but do not otherwise alter the circuit's characteristics.
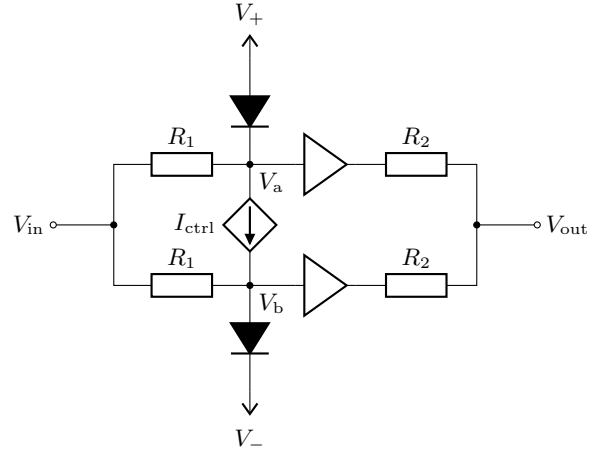

Figure 9: *Simplified circuit based on the VCA sections used in the Dolby A301 Audio Noise Reduction System's compressor modules.*

explicit expressions for each node,

$$V_{\text{a}} = V_{\text{in}} - I_{\text{ctrl}} R_1 - I_{\text{S}} R_1$$
$$+ \eta V_{\text{T}} \, \omega\left(\frac{-V_{\text{in}} + I_{\text{ctrl}} R_1 + V_+}{\eta V_{\text{T}}} + \omega^{-1}\left(\frac{I_{\text{S}} R_1}{\eta V_{\text{T}}}\right)\right),$$

$$V_{\text{b}} = V_{\text{in}} + I_{\text{ctrl}} R_1 + I_{\text{S}} R_1$$
$$- \eta V_{\text{T}} \, \omega\left(\frac{V_{\text{in}} + I_{\text{ctrl}} R_1 + V_+}{\eta V_{\text{T}}} + \omega^{-1}\left(\frac{I_{\text{S}} R_1}{\eta V_{\text{T}}}\right)\right),$$

which we combine to obtain the solution

$$V_{\text{out}} = V_{\text{in}}$$
$$+ \frac{1}{2} \eta V_{\text{T}} \, \omega\left(\frac{-V_{\text{in}} + I_{\text{ctrl}} R_1 + V_+}{\eta V_{\text{T}}} + \omega^{-1}\left(\frac{I_{\text{S}} R_1}{\eta V_{\text{T}}}\right)\right)$$
$$- \frac{1}{2} \eta V_{\text{T}} \, \omega\left(\frac{V_{\text{in}} + I_{\text{ctrl}} R_1 + V_+}{\eta V_{\text{T}}} + \omega^{-1}\left(\frac{I_{\text{S}} R_1}{\eta V_{\text{T}}}\right)\right). \quad (15)$$

From this, we may observe that when all corresponding components are matched, the $I_{\text{ctrl}} R_1$ and $I_{\text{S}} R_1$ terms cancel completely and no control current feedthrough is present at the output.

As in Sec. 3, we make a series of substitutions to (15): $\alpha := (\eta V_{\text{T}})^{-1}$, $\beta := (I_{\text{ctrl}} R_1 + V_+)/\eta V_{\text{T}} + \omega^{-1}(I_{\text{S}} R_1/\eta V_{\text{T}})$, $x := V_{\text{in}}$, and $y := V_{\text{out}}$. We now arrive at the generalized DSP model

$$y(x) = x - \frac{1}{2}\alpha^{-1}\omega(\alpha x + \beta) + \frac{1}{2}\alpha^{-1}\omega(-\alpha x + \beta). \quad (16)$$

Perhaps unexpectedly, the small-signal gain and gain control parameterization equations for (16) are identical to those in Sec. 5.1, namely

$$A = \frac{1}{\omega(\beta) + 1}, \quad (12\text{b revisited})$$

$$\beta(A) = \omega^{-1}\left(\frac{1 - A}{A}\right). \quad (12\text{c revisited})$$

The signal sweep and harmonic distortion introduced by this model are shown in Column (b) of Fig. 8. Unlike the other topologies described in this paper, (16) is an odd function and thus symmetrical about x even when α is large; therefore, only odd harmonics are present, and the total distortion produced by this model is

significantly lower than by the other models for the same α value. When $A = {}^1\!/_2$ (*i.e.*, $\beta = 1$), $y(x) \approx {}^x\!/_2$ and the function is approximately linear; relative harmonic distortion increases as $A \to 0$ and $A \to 1$. For all finite α and β, $\lim_{x \to \pm\infty} \partial y/\partial x = {}^1\!/_2$.

6. FUTURE WORK

Possible next steps include characterizing how digital diode-based VCA models behave when used as a subcomponent in effects such as compressors, expanders, and dynamic filters. The model could also be extended to behave like a four-quadrant multiplier for ring modulation, as in [14]. In particular, the variable harmonic distortion, signal gain contribution, and control parameter feedthrough inherent in these models may have interesting and unexpected consequences when present in the feedback path of a larger filter.

Additional diode-based VCA topologies beyond those discussed in this paper have been observed in audio hardware; these present additional opportunities for virtual analog modelling.

This paper introduced a family of digital VCA models based on fixed nonlinearities with variable operating points with the form

$$y(x) = \alpha^{-1} f(\alpha x + \beta) - \alpha^{-1} f(\beta), \tag{17a}$$

$$A := \lim_{\alpha \to 0} \frac{\partial y}{\partial x} = f'(\beta), \tag{17b}$$

$$\beta(A) = \left[f'\right]^{-1}(A). \tag{17c}$$

Another avenue of future study is found in adapting this model to other variable gain electronic components such as transistors and vacuum tube diodes, "omega-like" functions such as $f(x) = \ln\left(1 + e^x\right)^{\|}$, and other nonlinearities used in waveshaping, e.g., $f(x) = \tanh^{-1}(x)$ and $f(x) = \sin x$.

7. CONCLUSIONS

In this work, we presented and analyzed a DSP model that emulates a diode-based VCA. We derived closed-form equations for the small signal gain and gain control parameter, and quantified the degree of harmonic distortion. We also provided practical considerations for real-time implementation, including methods to minimize control feedthrough, avoid non-removable singularities, and reduce aliasing. Finally, we introduced a family of topological variations with different gain and distortion characteristics. The models presented are suitable for real-time applications and have a pleasing musical effect. They may be used as standalone signal processors or as subcomponents in larger audio effects.

Sound samples and supplementary materials are available on this paper's companion site^{**}.

8. ACKNOWLEDGMENTS

$^{\|}$Nonlinearities with the form $\ln\left(1 + e^x\right)$ have been used in e.g., [23] to model triodes.

**https://corianderpines.org/publications/ dafx2025_diode_vca/

9. REFERENCES

[1] J. Angus-Whiteoak, "Analogue voltage controlled amplifiers/attenuators (VCAs): A gentle introduction," AES United Kingdom Section Event, July 23, 2024, Available: https://www.youtube.com/watch?v=Ec1hm129NLE.

[2] R. Elliott, "VCA techniques investigated," Elliott Sound Products, Dec. 2012, Available: https://sound-au.com/articles/vca-techniques.html.

[3] C. A. A. Wass, *Introduction to Electronic Analogue Computers*, Electronics and Waves Monographs, D .W. Fry, Ed. McGraw-Hill Book Co. Ltd., 1955.

[4] M. Wizorke, "Siemens Begrenzer-Kompressor-Verstärker aus der Reihe der Sitral-Tonstudiogeräte," *Sonderdruck aus der Siemens-Zeitschrift*, vol. 39, pp. 912–916, Aug. 1965, Available: https://archive.org/details/studio_Siemens_U273_Limiter.

[5] Dolby Laboratories Inc., London, UK, *Audio Noise Reduction System A301*, 1966, Available: https://archive.org/details/JL11202.

[6] The Neve Group of Companies, Melbourn, UK, *Neve 2254/E Limiter/Compressor, Schematic B185/A*, 1974, Available: https://archive.org/details/neve-2254-schematics.

[7] AMS Neve PLC, Burnley, UK, *33609/J Limiter/Compressor Technical Handbook*, 3rd edition, 2002, Available: https://archive.org/details/neve-33609-j-technical-handbook.

[8] J. Schattschneider and U. Zölzer, "Discrete-time models for nonlinear audio systems," in *Proc. 2nd COST G-6 Workshop on Digital Audio Effects (DAFx99)*, Trondheim, Norway, Dec. 9-11, 1999.

[9] S. D'Angelo, L. Gabrielli, and L. Turchet, "Fast approximation of the Lambert W function for virtual analog modelling," in *Proc. 22nd Intl. Conf. Digital Audio Effects (DAFx-19)*, Birmingham, UK, Sept. 2-6, 2019, pp. 1–7.

[10] R. C. D. Paiva, S. D'Angelo, J. Pakarinen, and V. Välimäki, "Emulation of operational amplifiers and diodes in audio distortion circuits," *IEEE Transactions on Circuits and Systems II: Express Briefs*, vol. 59, no. 10, pp. 688–692, Oct. 2012.

[11] F. Eichas and U. Zölzer, "Black-box modeling of distortion circuits with block-oriented models," in *Proc. 19th Intl. Conf. Digital Audio Effects (DAFx-16)*, Brno, Czech Republic, Sept. 5-9, 2016, pp. 39–45.

[12] K. Dempwolf, M. Holters, and U. Zölzer, "Discretization of parametric analog circuits for real-time simulations," in *Proc. 13th Intl. Conf. Digital Audio Effects (DAFx-10)*, Graz, Austria, Sept. 6-10, 2010, pp. 1–8.

[13] D. T. Yeh, J. Abel, and J. O. Smith, "Simulation of the diode limiter in guitar distortion circuits by numerical solution of ordinary differential equations," in *Proc. 10th Intl. Conf. Digital Audio Effects (DAFx-07)*, Bordeaux, France, Sept. 10-15, 2007, pp. 197–204.

[14] R. Hoffman-Burchardi, "Digital simulation of the diode ring modulator for musical applications," in *Proc. 11th Intl. Conf. Digital Audio Effects (DAFx-08)*, Espoo, Finland, Sept. 1-4, 2008, pp. 1–4.

[15] J. Parker, "A simple digital model of the diode-based ring-modulator," in *Proc. 14nd Intl. Conf. Digital Audio Effects (DAFx-11)*, Paris, France, Sept. 19-23, 2011, pp. 163–166.

[16] M. O. Thurston, "Diodes," *IRE Transactions on Education*, vol. 3, no. 4, pp. 128–133, 1960.

[17] R. M. Corless, G. H. Gonnet, D. E. G. Hare, D. J. Jeffrey, and D. E. Knuth, "On the Lambert W function," *Advances in Computational Mathematics*, vol. 5, no. 1, pp. 329–359, Dec. 1996.

[18] T.C. Banwell and A. Jayakumar, "Exact analytical solution for current flow through diode with series resistance," *Electronics Letters*, vol. 36, no. 4, pp. 291–292, Feb. 17, 2000.

[19] R. M. Corless and D. J. Jeffrey, "The Wright ω function," in *Artificial Intelligence, Automated Reasoning, and Symbolic Computation*, J. Calmet et al., Eds. Jan. 2002, pp. 76–89, Springer Verlag, AISC-Calculemus 2002, LNAI 2385.

[20] P. W. Lawrence, R. M. Corless, and D. J. Jeffrey, "Algorithm 917: Complex double-precision evaluation of the Wright ω function," *ACM Trans. Math. Softw.*, vol. 38, no. 3, Apr. 2012.

[21] J. Parker, V. Zavalishin, and E. Le Bivic, "Reducing the aliasing of nonlinear waveshaping using continuous-time convolution," in *Proc. 19th Intl. Conf. Digital Audio Effects (DAFx-16)*, Brno, Czech Republic, Sept. 5-9, 2016, pp. 137–144.

[22] P. Horowitz and W. Hill, *The Art of Electronics*, Cambridge University Press, 2nd edition, 1989.

[23] K. Dempwolf and U. Zölzer, "A physically-moticated triode model for circuit simulations," in *Proc. 14th Intl. Conf. Digital Audio Effects (DAFx-11)*, Paris, France, Sept. 19-23, 2011, pp. 257–264.